Available online at www.sciencedirect.com
SCIENCE DIRECT
Journal of Catalysis 237 (2006) 405–415
JOURNAL OF CATALYSIS
www.elsevier.com/locate/jcat

Study of an iron-manganese Fischer–Tropsch synthesis catalyst promoted with copper

Cheng-Hua Zhang [a,b], Yong Yang [a], Bo-Tao Teng [a], Ting-Zhen Li [a], Hong-Yan Zheng [a], Hong-Wei Xiang [a], Yong-Wang Li [a,*]

[a] *State Key Laboratory of Coal Conversion, Institute of Coal Chemistry, Chinese Academy of Sciences, Taiyuan 030001, People's Republic of China*
[b] *Graduate School of the Chinese Academy of Sciences, Beijing 100039, People's Republic of China*

Received 7 June 2005; revised 2 November 2005; accepted 3 November 2005

Abstract

The metal–silica interaction and catalytic behavior of Cu-promoted Fe–Mn–K/SiO_2 catalysts were investigated by temperature-programmed reduction/desorption (TPR/TPD), differential thermogravimetric analysis, in situ diffuse reflectance infrared Fourier transform analysis, and Mössbauer spectroscopy. The Fischer–Tropsch synthesis (FTS) performance of the catalysts with or without copper was studied in a slurry-phase continuously stirred tank reactor. The characterization results indicate that several kinds of metal oxide–silica interactions are present on Fe–Mn–K/SiO_2 catalysts with or without copper, which include iron–silica, copper–silica, and potassium–silica interactions. In addition to the well-known effect of Cu promoter on easing the reduction of iron-based FTS catalysts, it is found that Cu promoter can increase the rate of carburization, but does not vary the extent of carburization during the steady-state FTS reaction. The basicity of the Cu and K co-promoted catalyst is greatly enhanced, as demonstrated by CO_2-TPD results. In the FTS reaction, Cu improves the rate of catalyst activation and shortens the induction period, whereas the addition of Cu has no apparent influence on the steady-state activity of the catalyst. Promotion of Cu strongly affects hydrocarbon selectivity. The product distribution shifts to heavy hydrocarbons, and the olefin/paraffin ratio is enhanced on the catalyst due to the indirect enhancement of surface basicity by the copper promotion effect.

Keywords: Fischer–Tropsch synthesis; Fe–Mn catalyst; Copper promotion; Metal–support interaction

1. Introduction

Fischer–Tropsch synthesis (FTS) has been recognized as an important technology in the production of liquid fuels and chemicals from syngas derived from coal, natural gas, and other carbon-containing materials. Following successfully applying FTS technologies at large scale by SASOL and Shell, energy industries are considering using this technology as an alternative route to compensate the depleting resources of crude oil [1]. In FTS process technology, a high-performance catalyst plays an essential role in industrial applications [1,2]. Among several options, Fe–Mn FTS catalysts have attracted much attention due to their high olefin selectivity and excellent stability [3–7]. Similar to the industrialized Fe–Cu–K catalyst, chemical promoters such as K_2O and Cu [5,8–16] were introduced into Fe–Mn catalysts to improve the activity and selectivity [17]. For the catalyst used in a slurry phase FTS reactor, structural promoters (silica, alumina, or other support materials) are also essential to improve attrition resistance and stability [18]. However, structural promoters were found to restrain the reducibility and decrease the activity due to the metal–support interaction [19]. It is well known that copper can facilitate the reduction at low temperature and improve the formation of FTS active phase [11–15]. Cu is thus often used to improve the catalyst performance and offset disadvantages of structure promoters for Fe-based catalysts. Although the function of copper in facilitating catalyst reduction has been widely accepted, its influence on FTS product distribution has not been well addressed. Wachs et al. [16] and O'Brien et al. [15] observed that copper had no effect

* Corresponding author. Fax: +86 351 4050320.
E-mail addresses: zhangchh@sxicc.ac.on (C.-H. Zhang), ywl@sxicc.ac.cn (Y.-W. Li).

0021-9517/$ – see front matter
doi:10.1016/j.jcat.2005.11.004

on product selectivity; this was established by conducting the FTS reaction in both differential fixed-bed and slurry-phase reactors. Bukur et al. [20] reported that incorporating Cu into iron-based catalysts resulted in an increase in the average molecular weight of hydrocarbon products; however, Li et al. [12] reported high CH_4 selectivity on a Cu-promoted Fe–Zn catalyst. Although a large number of studies were carried out on the influence of copper on FTS selectivity, controversy persists, because these studies were conducted under different conditions or over different catalyst systems. Therefore, further investigation is needed to illustrate the intrinsic relationship between Cu promoter and the FTS selectivity.

A metal oxide–support interaction on supported iron-based catalysts has been well discussed in the literature [14,19–22]. Bukur et al. [20] observed that supported Fe–Cu–K–SiO_2 catalysts produced less methane and gaseous hydrocarbons than unsupported catalyst. They ascribed this to the possibility of an Fe–SiO_2 (metal–support) interaction. However, most of these studies focused on the interaction between iron and the support, and little work has been done on the interaction between promoters present in relatively low levels and the support. The complex nature of the interaction between metal (Fe, Cu, K) oxides and the support in the catalyst, especially in multicomponent catalysts, makes it difficult to gain more insight into this interaction. Various techniques, including X-ray diffraction, X-ray photoelectron spectroscopy, scanning electron microscopy, and transmission electron microscopy, have failed to characterize the interaction between the low-level promoters and the support. Temperature-programmed reduction (TPR) is a useful method for studying the nature of the metal–support interaction [6,14,23]. However, in previous reports [5,14,23], little information on the promoter–support interactions was provided by TPR.

The present study focuses on the effect of copper on the catalytic performance of a co-precipitated Fe–Mn catalyst (FeMnCuK/SiO_2). Because of the complexity of the metal oxide–support interactions, several techniques, including H_2-TPR, H_2-differential thermogravimetric analysis (DTG), CO_2-temperature-programmed desorption (TPD), and in situ diffuse reflectance infrared Fourier transform spectroscopy (DRIFTS), were used together to characterize the interaction between these components in the catalyst and to illustrate the function of copper in the catalyst. To characterize the interaction, three model catalysts (Si-free, K-free, and CuK-free catalysts) were also used. In addition, H_2-TPD, CO-TPR, Mössbauer spectroscopy, and slurry-phase FTS reaction measurements were performed to investigate the reduction, carburization, and FTS performance of catalysts.

2. Experimental

2.1. Catalyst preparation

Two catalyst samples, Cu-free and Cu-promoted FeMnK/SiO_2 catalysts, were used in this work. The catalysts were prepared using the combination of coprecipitation and spray drying. A solution containing $Fe(NO_3)_3$ (99.9+%; Tianjin Chemical Co., PR China), $Mn(NO_3)_2$ (99.9+%; Tianjin Chemical Co.), $Cu(NO_3)_2$ (99.9+%; Tianjin Chemical Co.), and silica gel (SiO_2, 30.0%; Tianjin Chemical Co.) with an Fe/Mn/Cu/SiO_2 weight ratio of $100/12/x/15$ ($x = 0$ or 1) was introduced into a 20 l precipitation vessel containing deionized water (∼1 l) at 350 ± 1 K. A NH_4OH solution (Tianjin Chemical Co.) was added simultaneously into this precipitation vessel to maintain the pH at a constant value of 9.0 ± 0.1, as measured with a pH meter (PHS-25; Shanghai Leici Co., PR China). After precipitation, the precipitate was filtered. A K_2CO_3 (99.9+%, Tianjin Chemical Co.) solution and deionized water in the amounts required to obtain the desired K/Fe weight ratio of 3/100 were added to the filter cake, and the mixture was then reslurried and spray-dried. The obtained catalyst precursors were calcined at 773 K for 5 h. The final obtained catalysts were composed of 100 Fe/10 Mn/3 K/12 SiO_2 (FeMnK/SiO_2) and 100 Fe/10 Mn/3 K/1 Cu/12 SiO_2 (FeMnCuK/SiO_2) in mass ratio, respectively. In addition, an unpromoted model catalyst with a composition of 100 Fe/10 Mn/12 SiO_2 (FeMn/SiO_2), a silica-free model catalyst with a composition of 100 Fe/10 Mn/3 K/1 Cu (FeMnCuK), and a potassium-free model catalyst with a composition of 100 Fe/10 Mn/1 Cu/12 SiO_2 (FeMnCu/SiO_2) were prepared to study the metal–silica interaction or the surface basicity.

2.2. Catalyst characterization

2.2.1. TPR

TPR experiments were performed in an atmospheric quartz tube flow reactor (5 mm i.d.). A flow of 5% H_2 in Ar or 5% CO in He was used as the reduction gas. A part of the effluent stream in H_2-TPR was connected to a quadrupole mass spectrometer (OmniStar 200; Balzers, Switzerland) to measure the concentration of H_2. The effluent stream in CO-TPR was connected to a gas chromatograph using a thermal conductivity detector (TCD) to monitor the variation of CO concentration. An in-line drierite trap (in the H_2-TPR mode) or a liquid-nitrogen trap (in the CO-TPR mode), located between the reactor and the MS/TCD, was used to continuously remove water or CO_2 produced during reduction. Typically, 80 mg of catalyst was loaded into the quartz tube reactor and reduced by raising the temperature from 373 to 1273 K.

A second-run H_2-DTG was performed using a TGA92 thermogravimetric system (Setaram, France) with a flow of 5% H_2 in Ar or 5% O_2 in Ar as the reduction gas or the oxidation gas. A 20-mg catalyst sample was loaded into the thermal balance reactor. The second-run H_2-DTG was carried out with following program. First, the catalyst was reduced by raising the temperature from room temperature to 773 K and holding it there for 30 min; this was the first run of H_2-DTG. In the second run of H_2-DTG, the reduced catalyst was purged with Ar, cooled to room temperature in Ar, and reoxidized with the same temperature program used in the first run. Finally, the reoxidized catalyst was reduced identically as in the first run.

The H_2- and CO_2-TPD experiments were performed in the same system as used in TPR, with Ar (in H_2-TPD) or He (in CO_2-TPD) as the carrier gas. The effluent was measured by gas

chromatography using a TCD. A 200-mg catalyst sample was loaded in the reactor. Note that, particularly for the H_2-TPD experiments, the catalyst was first reduced with H_2 at 773 K and 0.1 MPa for 10 h. Then the sample was heated in the carrier gas from 323 to 773 K, held at 773 K until the baseline leveled off (ensuring complete removal of adsorbed species on the reduced catalyst surface), and finally cooled to 323 K for the TPD tests. In the subsequent steps, H_2 or CO_2 adsorption on catalyst was performed at 323 K for 30 min, and then the sample was purged with the carrier gas for 30 min to remove weakly adsorbed species. After this step, H_2- or CO_2-TPD was carried out while the temperature was increased to 773 K. H_2 chemisorption uptakes were determined by integrating the area of H_2-TPD curves and comparing them with those of known amounts of the gas passed through the TCD.

In the temperature-programmed process, the reducing or carrier gases were introduced into a series of desulfurizing agent, molecular sieves, and silica gel traps to remove impurities. The gas flow was maintained at 50 ml/min, and the temperature ramp was set at 10 K/min.

2.2.2. DRIFTS analysis

DRIFTS spectra were collected using an infrared spectrometer (Equinox55, Bruker, Germany), equipped with KBr optics and a MCT D316 detector at the liquid nitrogen temperature (77 K). The infrared cell with ZnSe windows was connected to a feed system with a set of stainless steel gas lines, allowing in situ measurements for the adsorption of probe molecules. CO_2 and Ar were used as probe molecule and flushing gas, respectively. The spectra were collected before and after CO_2 adsorption. In all cases, the gas flow was maintained at 50 ml/min. All spectra were recorded with a resolution of 4 cm^{-1} and accumulation of 64 scans.

2.2.3. Mössbauer spectroscopy

The Mössbauer spectra of catalysts were recorded at 4.4 K using a CANBERRA Series 40 MCA constant-acceleration Mössbauer spectrometer and a 25-mCi ^{57}Co in Pd matrix. The spectrometer was operated in the symmetric constant acceleration mode. The spectra were collected over 512 channels in mirror-image format. Data analysis was performed using a nonlinear least squares fitting routine that models the spectra as a combination of singlets, quadruple doublets, and magnetic sextets based on a Lorentzian line shape profile. The spectral components were identified based on their isomer shift (δ), quadruple splitting (Δ), and magnetic hyperfine field (Hhf). All isomer shift values were reported with respect to metallic iron (α-Fe) at the measurement temperature. Magnetic hyperfine fields were calibrated with the 330-kOe field of α-Fe at ambient temperature.

2.2.4. Surface area measurements

BET surface area measurements were carried out before and after reduction. N_2 physisorption measurements were performed at its normal boiling point (77 K) using a Micromeritics ASAP 2500, and surface areas were calculated using the BET method.

2.3. FTS

The FTS performance of the catalysts was tested in a 1-dm^3 continuously slurry stirred tank reactor loaded with 20.0 g of catalyst sample and 380 g of liquid paraffin.

The H_2 and CO were passed separately through a series of purification traps to remove trace amounts of iron carbonyls, water, and other impurities. The flow rates of H_2 and CO were controlled by two mass flow controllers (Brooks, model 5850E). The exit stream passed through a hot trap (393 K), a back-pressure regulator, and a cold trap (273 K) to collect liquid products. A wet gas flow meter was used to monitor the flow rate of tail gas.

The catalyst was reduced in situ in syngas ($H_2/CO = 0.67$) at 553 K, 0.50 MPa, and 1000 h^{-1} for 80 h. After reduction, steady-state reaction conditions were set as 523 K, 1.5 MPa, $H_2/CO = 0.67$, and 2000 h^{-1}.

The tail gas was analyzed online by gas chromatography (GC) (models 6890N and 4890D; Agilent) equipped with a 16-port sampling valve and two sampling loops. In one sampling loop, the hydrocarbons were analyzed with an Al_2O_3 capillary column (HP-PLOT, 30 m × 0.53 mm) and a flame ionization detector (FID). In the other loop, H_2, N_2, CO, CO_2, and CH_4 were analyzed with a Porapak Q stainless steel packed column (2 m × 3 mm), a PLOT Q packed column (HP-PLOT, 25 m × 0.53 mm), a molecular sieve 5A packed column (HP-PLOT, 30 m × 0.53 mm), and a TCD. The products in oil phase were analyzed off-line by GC (model 6890N, Agilent) with a quartz capillary column (DB-1, 60 m × 0.25 mm) and an FID. The products in wax were analyzed offline using a gas chromatograph (6890N, Agilent, USA) with a stainless steel capillary column [UA^+-(HT), 30 m × 0.53 mm] and an FID. Oxygenates in water were analyzed off-line using GC (model 6890N; Agilent) with a quartz capillary column (J&W DB-WAX, 30 m × 0.32 mm) and an FID.

3. Results and discussion

3.1. H_2-TPR and H_2-DTG

H_2-TPR was used to investigate the effect of Cu on the reduction behavior of the Fe–Mn catalysts. Fig. 1 shows H_2-TPR profiles of three catalysts (FeMnK/SiO_2, FeMnCuK/SiO_2, and FeMnCuK). The unsupported catalyst (FeMnCuK) demonstrates several peaks in the H_2-TPR profile. The H_2-TPR profile of the FeMnCuK/SiO_2 catalyst is generally similar to that of the FeMnCuK catalyst; however, the overall TPR profile of former is obviously narrowed, due to the existence of the silica support. Therefore, reduction for the FeMnCuK/SiO_2 catalyst starts at higher temperature and finishes at lower temperature compared with that for the FeMnCuK catalyst. For the catalyst without Cu promoter, FeMnK/SiO_2, the low-temperature TPR profile shows a broad peak, and the whole reduction process ends at the same temperature as for the FeMnCuK catalyst.

The amount of H_2 consumed during different reduction stages, obtained from integrating the area of the corresponding reduction peak, is summarized in Table 1. For the FeMnCuK

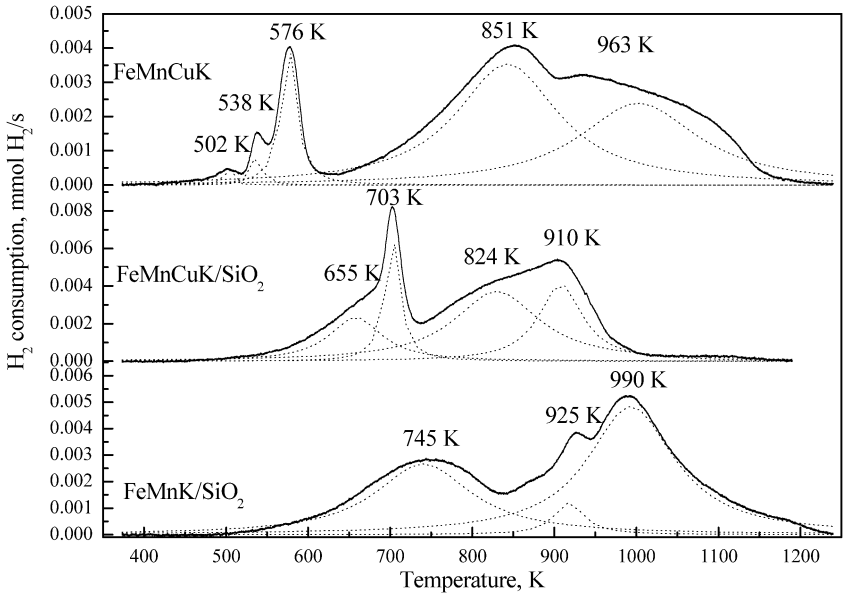

Fig. 1. H_2-TPR profiles for $FeMnK/SiO_2$, $FeMnCuK/SiO_2$, and FeMnCuK catalysts. (—) Experimental curves; (···) Lorentzian multi-peak fitting curves.

Table 1
Quantitative results of H_2 consumption for $FeMnK/SiO_2$, $FeMnCuK/SiO_2$, and FeMnCuK catalysts in H_2-TPR[a]

Catalysts	Peak (K)	H_2 consumption	
		mol H_2/mol M[b]	mol H_2/mol Fe
$FeMnK/SiO_2$	745	0.54	
	925		0.07
	990		0.89
$FeMnCuK/SiO_2$	655	0.26	
	703	0.20	
	824		0.67
	910		0.38
FeMnCuK	502	0.001	
	538	0.02	
	576	0.12	
	851		0.76
	963		0.60

[a] The H_2 consumption was measured from the area under the corresponding peak.
[b] M = Fe + Mn + Cu.

catalyst, the overall H_2 consumption [0.141 mol H_2/mol M (Fe + Mn + Cu)] of reduction peaks at 502, 538, and 576 K is < 0.15 mol H_2/mol M. These peaks can be assigned to the reduction of CuO, α-Mn_2O_3, and α-Fe_2O_3 to Cu, MnO, and Fe_3O_4, respectively. The peaks at 851 K (0.76 mol H_2/mol Fe) and 963 K (0.60 mol H_2/mol Fe) correspond to the reduction of Fe_3O_4 to Fe. For two silica-supported catalysts, the amounts of H_2 consumption for reduction peaks at lower temperature range (600–800 K) (0.54 mol H_2/mol M for $FeMnK/SiO_2$ and 0.46 mol H_2/mol M for $FeMnCuK/SiO_2$) are close to the theoretical value for the reduction of metal oxides to Cu, MnO, and FeO (0.56 mol H_2/mol M). The peaks at higher temperature (above 800 K) correspond to the reduction of FeO to Fe, and the H_2 consumptions are consistent with theoretical values.

It is clearly shown that the iron oxides in all of the catalysts can be completely reduced to α-Fe in TPR process for temperatures up to 1000 K. In addition, there are some obvious differences in the TPR profiles of these catalysts. First, the phase transformations of the unsupported catalyst during TPR process are CuO → Cu, Mn_2O_3 → MnO, and Fe_2O_3 → Fe_3O_4 → α-Fe, whereas those of supported catalysts ($FeMnK/SiO_2$ and $FeMnCuK/SiO_2$) are CuO → Cu, Mn_2O_3 → MnO, and Fe_2O_3 → FeO → α-Fe, in which the reduction of α-Fe_2O_3 occurs via wüstite (FeO) as an intermediate phase rather than Fe_3O_4 [6]. Wüstite is a metastable phase of iron oxides below 843 K [24]. Many studies [25–27] have reported that FeO is observed on the supported catalysts. It can be reasoned that FeO is stabilized by the support [6,25–27]. Second, there are three well-defined reduction peaks at low temperatures in the TPR profile of the FeMnCuK catalyst corresponding to the reduction of CuO, Mn_2O_3, and Fe_2O_3. But these reduction peaks overlap into a broad peak on $FeMnK/SiO_2$ and $FeMnCuK/SiO_2$ catalysts, and the required temperatures are also apparently increased, suggesting that the addition of silica suppresses the reduction of metal oxides. Third, the peak at high temperature in the TPR of the $FeMnCuK/SiO_2$ catalyst is narrower than that of the FeMnCuK catalyst, suggesting that the iron oxide on Si-supported and Cu-promoted catalyst is more easily reduced to α-Fe at high temperatures than that on unsupported catalyst. A possible reason for this phenomenon is that the iron oxide is highly dispersed on the silica support, preventing the aggregation of crystallites and favoring the reduction of the iron oxide at high temperature. Finally, the temperature needed for reduction is lower for the $FeMnCuK/SiO_2$ catalyst than for the $FeMnK/SiO_2$ catalyst, indicating that Cu improves the reducibility of metal oxides. This may result from the high probability of H_2 dissociation of copper [28] and the interaction between copper and iron. Hence an interaction between metal oxides and the silica support can be envisioned in which

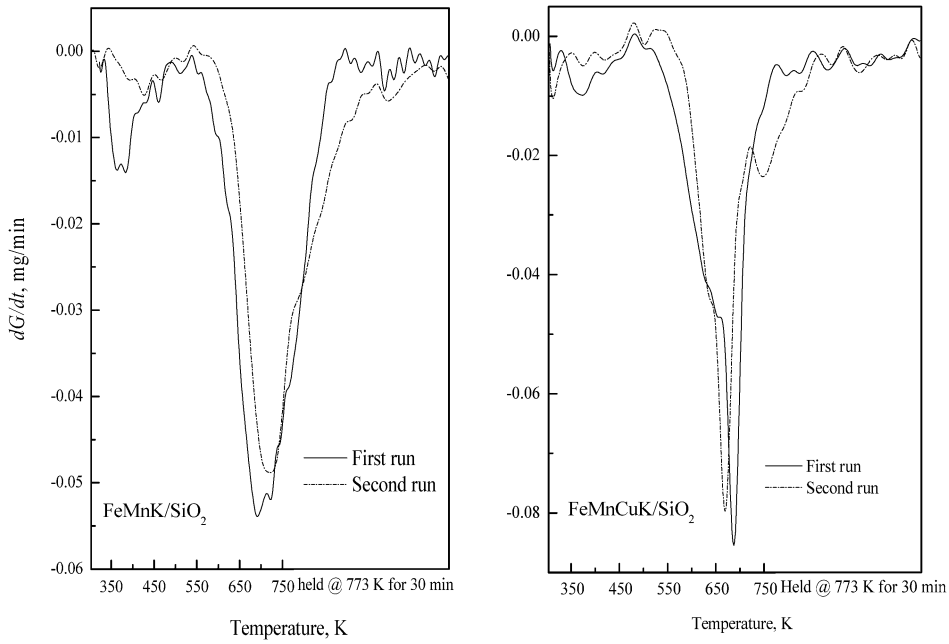

Fig. 2. Second-run H_2-DTG profiles for $FeMnK/SiO_2$ and $FeMnCuK/SiO_2$ catalysts. (—) The first run of H_2-DTG, and (·····) the second run of H_2-DTG after completion of the first run and catalyst reoxidation at 773 K for 30 min.

the interaction suppresses the reduction of metal oxides at low temperature. On the other hand, the dispersion effect of the silica support prevents the aggregation of iron crystallites, improving the reduction of iron oxide. Although the interaction between copper and silica suppresses the reduction of CuO to some extent, the high probability of H_2 dissociation of Cu can still facilitate the reduction of Fe_2O_3.

The H_2-TPR results provide evidence for the interaction between copper and silica to some extent. A second-run H_2-DTG further confirms this kind of interaction. The second-run H_2-DTG profiles for the $FeMnK/SiO_2$ and $FeMnCuK/SiO_2$ catalysts, shown in Fig. 2, reveal that the reduction of metal oxides occurs in the temperature range of 550–773 K. The reduction peak of $FeMnCuK/SiO_2$ in the first run is sharper than that of $FeMnK/SiO_2$, indicating that copper improves the reduction rate. For the $FeMnK/SiO_2$ catalyst, the onset of reduction and the temperature at which the reduction rate is at a maximum are delayed in the second run compared with the first run, possibly due to the aggregation of metal oxides in the first run and also to a reoxidation process. For the $FeMnCuK/SiO_2$ catalyst, in the second run the onset of reduction is slower, but the peak is earlier, than in the first run. In addition, there a weak peak occurs at high temperature that may represent the further reduction of iron oxides (FeO_x to α-Fe). The delayed peak onset indicates that particles of metal oxide aggregate after the first run and reoxidation, whereas the advanced peak maximum and the minor peak at high temperature indicate that the reduction of the $FeMnCuK/SiO_2$ catalyst becomes easier after the first run and reoxidation. Clearly, Cu promotion not only improves the reduction of metal oxides in the first run, but also further decreases the temperature required for reduction in the second run. This indicates that the effective Cu content in $FeMnCuK/SiO_2$ increases after the first run and reoxidation. The only source of the increased effectiveness of Cu is the copper–silica interaction. We suggest that copper in the precipitated $FeMnCuK/SiO_2$ catalyst interacts partly with metal (Fe and Mn) oxides and partly with silica. The former can improve the reduction of metal oxides, but the latter cannot. In the second run of the H_2-DTG, the latter part segregates from the silica during reduction in the first run. The released Cu reinteracts with metal (Fe and Mn) oxides and further improves the reduction of metal oxides in the second run. Therefore, the second-run H_2-DTG provides evidence for the existence of copper–silica interaction in the $FeMnCuK/SiO_2$ catalyst.

3.2. CO_2 adsorption on catalysts

The CO_2-TPD curves of $FeMnK/SiO_2$, $FeMnCuK/SiO_2$, $FeMnCu/SiO_2$, and $FeMn/SiO_2$ catalysts are shown in Fig. 3. The CO_2 uptakes can be used as indicators of the intensity and strength of surface basic sites on catalysts. As shown in Fig. 3, there are several peaks in the TPD profiles. A small peak (peak 1) at about 373 K and a long tail (peak 4) at temperature above 620 K are present in all of the profiles. The small peak at low temperature corresponds to the desorption of CO_2 weakly adsorbed in bulk phase. The tail above 620 K is probably from the slow decomposition of a small amount of metal carbonates formed during CO_2 adsorption or catalyst preparation. Two intense and broad peaks in the temperature range of 400–650 K are present in the TPD profiles of $FeMnK/SiO_2$ and $FeMnCuK/SiO_2$ catalysts, corresponding to the desorption of CO_2 that interacts moderately with the surface basic sites. In a detailed analysis, the profiles of $FeMnCu/SiO_2$ and $FeMn/SiO_2$ catalysts resemble each other, and no apparent peak appears in the temperature range of 400–650 K. The strong desorption peaks 2 and 3 appear in the profiles of $FeMnK/SiO_2$ and

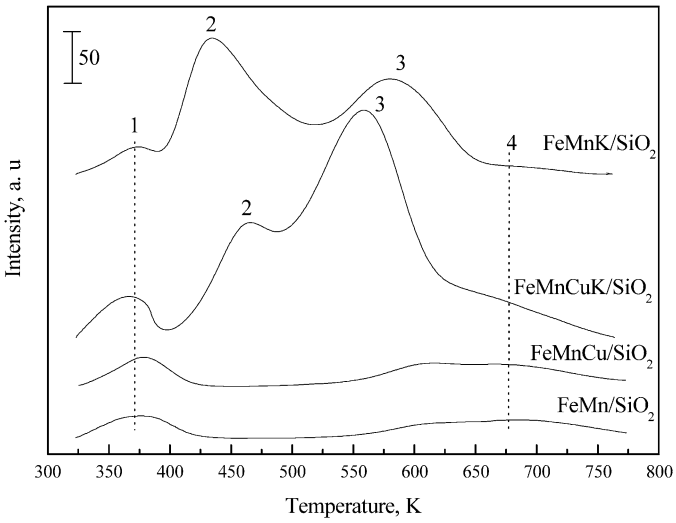

Fig. 3. CO_2-TPD profiles of $FeMnK/SiO_2$, $FeMnCuK/SiO_2$, $FeMnCu/SiO_2$, and $FeMn/SiO_2$ catalysts.

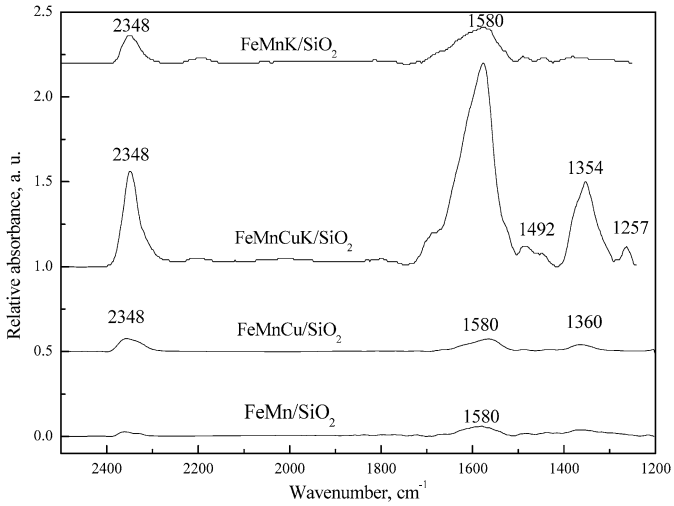

Fig. 4. IR spectra recorded from CO_2 adsorption at 473 K on $FeMnK/SiO_2$, $FeMnCuK/SiO_2$, $FeMnCu/SiO_2$, and $FeMn/SiO_2$ catalysts in situ calcined at 773 K. Each spectrum is reported as the difference between the spectra before and after CO_2 admission.

$FeMnCuK/SiO_2$ catalysts, indicating that potassium plays a critical role in improving the surface basicity. Because peaks 2 and 3 are present only for the potassium-promoted catalysts, the basic sites in these catalysts can be attributed mainly to the potassium species on catalyst surfaces, implying that the basicity is mainly from K-basic sites. These K-basic sites with different CO_2 desorption temperatures represent different chemical states of potassium on the catalyst surfaces. Dry et al. [29] reported that alkali silicates are less basic and alkali oxides are more basic. Therefore, these different chemical states of potassium may result from the interactions of potassium and silica (with TPD peak 2) and potassium and oxygen (peak 3). Compared with the $FeMnK/SiO_2$ catalyst, for the $FeMnCuK/SiO_2$ catalyst, peak 2 becomes weaker and shifts to higher temperature and peak 3 becomes stronger and shifts to lower temperature. In addition, the total area of the TPD profile of $FeMnCuK/SiO_2$ is 1.5 times larger than that of $FeMnK/SiO_2$. These results indicate that Cu counteracts the strength of two types of K-basic sites and increases the amounts of the total basic sites.

The effect of copper on surface basicity can be further proved by DRIFTS analysis. Infrared spectra of CO_2 adsorption on catalysts are presented in Fig. 4. On $FeMnK/SiO_2$, $FeMnCuK/SiO_2$, $FeMnCu/SiO_2$, and $FeMn/SiO_2$ catalysts, several bands at 2348, 1580, 1450, 1355, and 1257 cm^{-1} appear after CO_2 adsorption. These bands can be assigned to the carbonates formed on surface basic sites [30–36]. Comparing the spectra of the four samples, the intensity of carbonate bands on $FeMn/SiO_2$ and $FeMnCu/SiO_2$ catalysts is very weak, whereas the bands at 2348 and 1580 cm^{-1} are enhanced to some extent on the $FeMnK/SiO_2$ catalyst with promotion of potassium. For the $FeMnCuK/SiO_2$ catalyst, all of the bands of carbonates are apparently enhanced with the promotion of copper promoter. These results indicate that the Cu and K co-promoted catalyst ($FeMnCuK/SiO_2$) has more surface basic sites than the unpromoted and separately Cu- or K-promoted catalysts ($FeMn/SiO_2$, $FeMnCu/SiO_2$, and $FeMnK/SiO_2$).

The analysis of CO_2-TPD and DRIFTS results reveals that several kinds of basic sites are present on the unpromoted $FeMn/SiO_2$ catalyst, although the amount of basic sites is low. Promotion of potassium can apparently improve the surface basicity of catalysts ($FeMnK/SiO_2$ and $FeMnCuK/SiO_2$). With only Cu present as a promoter ($FeMnCu/SiO_2$), the surface basicity is similar to that of unpromoted catalyst ($FeMn/SiO_2$), whereas a synergistic effect is observed on Cu and K co-promoted catalyst ($FeMnCuK/SiO_2$), which has a moderate strength of basicity and more basic sites than K-promoted catalyst ($FeMnK/SiO_2$). A possible reason for the synergistic effect is that, although potassium is the main source of surface basic sites, the interaction between potassium and silica suppresses the intrinsic basicity of potassium on the $FeMnK/SiO_2$ catalyst, decreasing the amount of effective potassium [8]. With the addition of copper into the catalyst, the copper–silica interaction weakens the potassium–SiO_2 interaction, leading to the increase of the amount of effective potassium on the catalyst surface. Thus, the surface basicity is indirectly improved by Cu promotion on the Cu and K co-promoted catalyst ($FeMnCuK/SiO_2$).

3.3. Reduction and carburization behaviors

As mentioned in H_2-TPR, copper can facilitate the reduction of metal oxides in H_2. Table 2 shows the BET surface area and H_2 chemisorption uptakes on $FeMnK/SiO_2$ and $FeMnCuK/SiO_2$ catalysts after reduction with 5% H_2 in Ar at 773 K for 10 h. BET surface areas are nearly identical for $FeMnK/SiO_2$ and $FeMnCuK/SiO_2$ catalysts before reduction, indicating that the presence of a small amount of Cu does not affect the textural structure of catalyst precursors. After H_2 reduction, the BET surface area of $FeMnCuK/SiO_2$ is slightly higher than that of $FeMnK/SiO_2$. The H_2 uptake is also higher on $FeMnCuK/SiO_2$ than on $FeMnK/SiO_2$, indicating that the presence of copper improves the reduction rate of the catalyst

Table 2
H_2 uptakes on reduced FeMnK/SiO_2 and FeMnCuK/SiO_2 catalysts

Catalysts		FeMnK/SiO_2	FeMnCuK/SiO_2
Surface area (m^2/g)	Before reduction	197.42	201.25
	After reduction[a]	98.38	107.92
H_2 uptake[b] ($\times 10^{-2}$ mmol H_2/mmol Fe)		5.00	8.95

[a] The BET surface area was measured after exposure to 5% H_2 in Ar at 773 K for 10 h (0.2 g sample, gas flow rate = 50 ml/min).

[b] The H_2 uptake on catalysts was determined by integrating the area under the H_2-TPD curves.

and restricts the aggregation of Fe crystallites, resulting greater surface area, smaller crystal particles, and a larger number of H_2 adsorptive sites after the reduction in H_2.

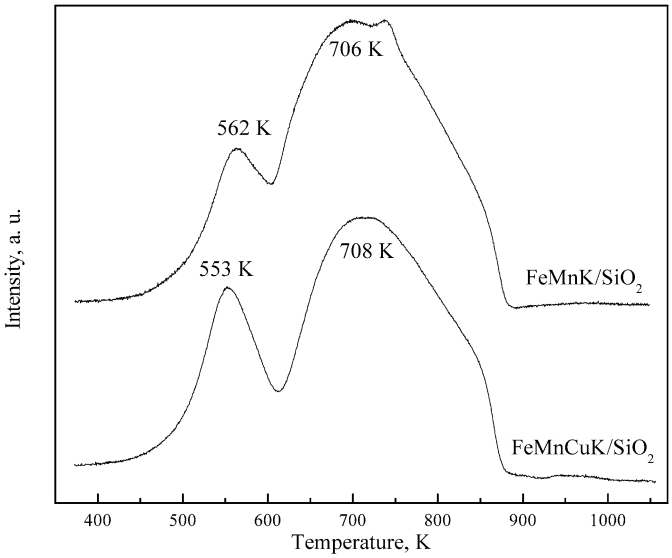

Fig. 5. CO-TPR profiles of FeMnK/SiO_2 and FeMnCuK/SiO_2 catalysts.

Fig. 5 shows the CO-TPR profiles of the FeMnK/SiO_2 and FeMnCuK/SiO_2 catalysts. Under CO atmosphere, the catalyst is reduced and carburized via two steps, hematite (Fe_2O_3) to magnetite (Fe_3O_4) and magnetite to iron carbides [37–40]. The promotion of Cu slightly decreases the reduction temperature of Fe_2O_3 to Fe_3O_4 and apparently increases the removal rate of oxygen; however, the carburization peaks of the two catalysts appear to be identical, indicating that Cu does not apparently affect the extent of carburization.

Fig. 6 shows the isothermal reduction behavior of FeMnK/SiO_2 and FeMnCuK/SiO_2 catalysts in syngas. The CO_2 concentration in the tail gas was used to monitor the reduction behavior. Note, however, that the reduction process using syngas for iron FTS catalysts is inevitably accompanied by the FTS reaction (typically methanation and the water–gas shift (WGS) reaction), even in very early stages of the reduction at normal pressure and the elevated temperature used as reduction conditions. In this case, CO_2 levels in tail gas qualitatively reflect the extent of iron reduction, and thus directly reflect the reduction of the catalyst.

As shown in Fig. 6, when the temperature was increased to 553 K and kept constant, the CO_2 concentration for the FeMnK/SiO_2 catalyst increased slowly from a low to a high level and then remained stable with increasing time on stream. However, that of the FeMnCuK/SiO_2 catalyst increased quickly to the maximum and declined slightly thereafter with increasing reduction time. The CO_2 concentration of FeMnCuK/SiO_2 is higher than that of FeMnK/SiO_2, indicating that the presence of Cu apparently enhances the reduction of catalyst in syngas.

Fig. 7 shows the Mössbauer spectra of FeMnK/SiO_2 and FeMnCuK/SiO_2 catalysts at different states in the FTS reaction. Table 3 lists the iron-phase composition of FeMnK/SiO_2 and FeMnCuK/SiO_2 catalysts, as determined by fitting the Mössbauer spectra. Although the FTS reaction does not occur in the

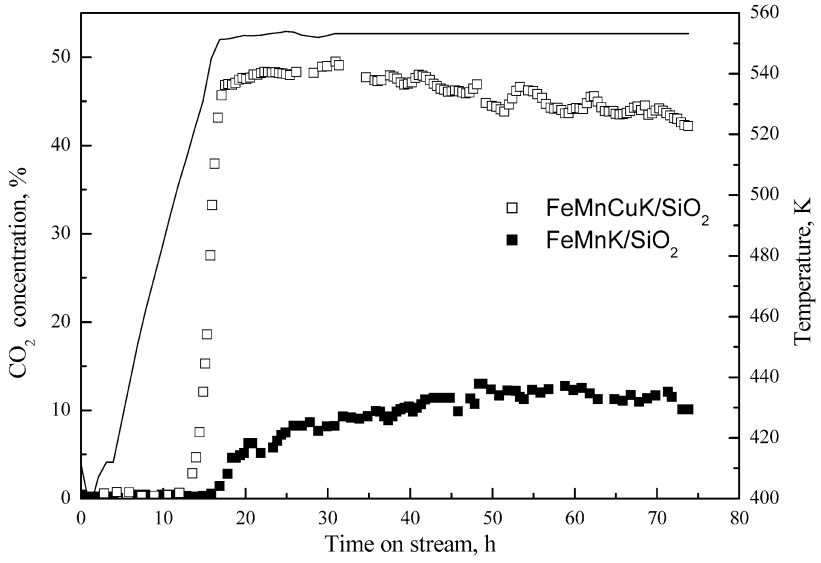

Fig. 6. In situ reduction behaviors of (■) FeMnK/SiO_2 and (□) FeMnCuK/SiO_2 catalysts in syngas; (—) reduction temperature; reduction conditions: 553 K, 0.5 MPa, 1000 h^{-1}, and $H_2/CO = 0.67$.

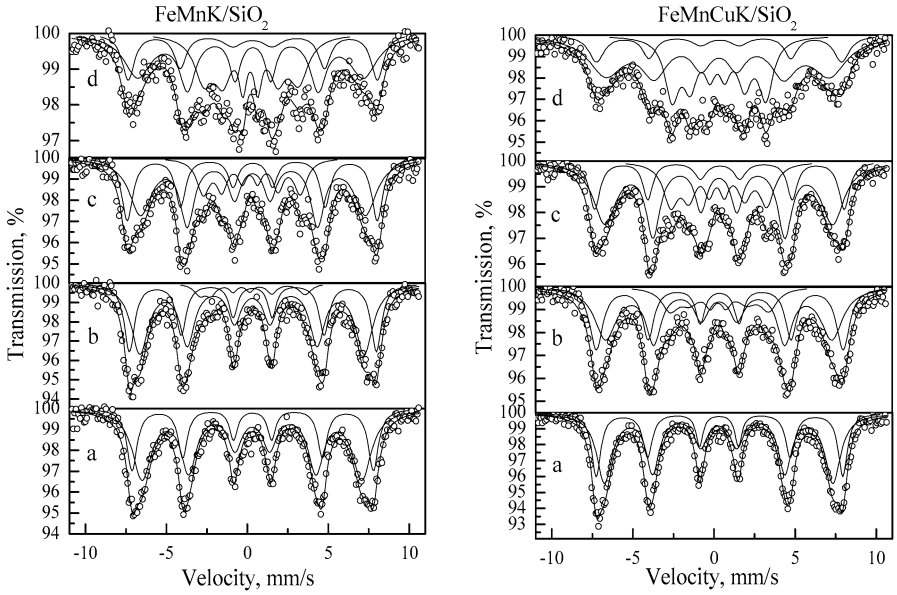

Fig. 7. Mössbauer spectra of FeMnK/SiO_2 and FeMnCuK/SiO_2 catalysts at different states: (a) as prepared, (b) after reduction, (c) reaction for 250 h, (d) reaction for 500 h.

Table 3
Iron phase composition of FeMnK/SiO_2 and FeMnCuK/SiO_2 catalysts in reduction or FTS reactions[a]

Catalysts	FeMnK/SiO_2		FeMnCuK/SiO_2	
	Phase	Area (%)	Phase	Area (%)
As-prepared	Fe_2O_3	68	Fe_2O_3	64.9
	Fe_2O_3	32	Fe_2O_3	35.1
After reduction	Fe_3O_4 (A)	34.7	Fe_3O_4 (A)	35.5
	Fe_3O_4 (B)	58.6	Fe_3O_4 (B)	48.5
	FeC_x	6.7	FeC_x	16.0
Reaction for 250 h	Fe_3O_4 (A)	29.1	Fe_3O_4 (A)	20.4
	Fe_3O_4 (B)	52.2	Fe_3O_4 (B)	55.2
	FeC_x	18.7	FeC_x	24.3
Reaction for 500 h	Fe_3O_4 (A)	21.8	Fe_3O_4 (A)	15.7
	Fe_3O_4 (B)	44.9	Fe_3O_4 (B)	51.1
	FeC_x	33.3	FeC_x	33.3

[a] The iron phase composition were determined using Mössbauer spectroscopy at liquid Helium temperature (4.4 K) with a γ-ray-transparent Be windows.

bulk phase of carbides, the carbides can have FTS-active sites on their surfaces. Thus, it is proposed that iron carbides are main active phases for FTS reactions [41–45], and their content can be used to monitor the formation of FTS active sites to some extent. As shown in Fig. 7 and Table 3, the content of iron carbides after reduction is almost threefold higher in the FeMnCuK/SiO_2 catalyst than in the FeMnK/SiO_2 catalyst, paralleling the difference in CO_2 concentration during in situ syngas reduction between two catalysts. The content of iron carbides in the FeMnCuK/SiO_2 catalyst during the FTS reaction (250 h) is also higher than that of the FeMnK/SiO_2 catalyst; however, the extent of carburization for the two catalysts after 500 h steady-state run is nearly identical. These results indicate that Cu promotion leads to higher rate of carburization but has no apparent influence on the final extent of carburization.

It was previously reported that the reduction of iron-based FTS catalyst can be enhanced by introducing copper as a promoter [11–15,19], and our experimental results confirm this. The reduction process of iron-based catalysts generally includes the removal of oxygen atoms from the metal oxide and carburization of the reduced (often partially reduced) surface (if CO is present in the reduction agent) [37–40,46]. This "reduction" stage is impossible to clearly distinguish from the whole reduction and FTS reaction procedure. Very often, the FTS reaction (methanation) and the WGS reaction start once the catalysts are partially reduced. However, in terms of copper's role in this initial stage of reduction (accompanying the FTS reaction), oxygen removal in the initial stage (reduction) is greatly promoted by introducing copper (Figs. 1 and 5), because copper oxide can be easily reduced to a metal state by reductants at low temperatures [14], and the metallic copper plays an essential role in helping the removal of oxygen atom from other oxide phases [46]. As for a mechanistic understanding, we infer that on the one hand, metallic copper facilitates the activation of the H_2 present in reducing agents, but on the other hand, metallic copper atoms, which are highly dispersed in the iron phase, may weaken vicinal Fe–O bonds. This latter mechanism may explain the copper promotion to the CO reduction cases. This mechanism provides insight into enhancement of the carburization rate of FTS catalysts by copper promoter, as indicated in Table 3, confirming that the major role of copper is to facilitate the reduction of metal oxides.

3.4. FTS performance

FTS performance of the FeMnK/SiO_2 and FeMnCuK/SiO_2 catalysts was measured under conditions of 543 K, 1.5 MPa, 2000 h^{-1}, and $H_2/CO = 0.67$. The activities and stabilities were first tested over a 500-h steady-state run, and then the selectivities were studied under various conversions.

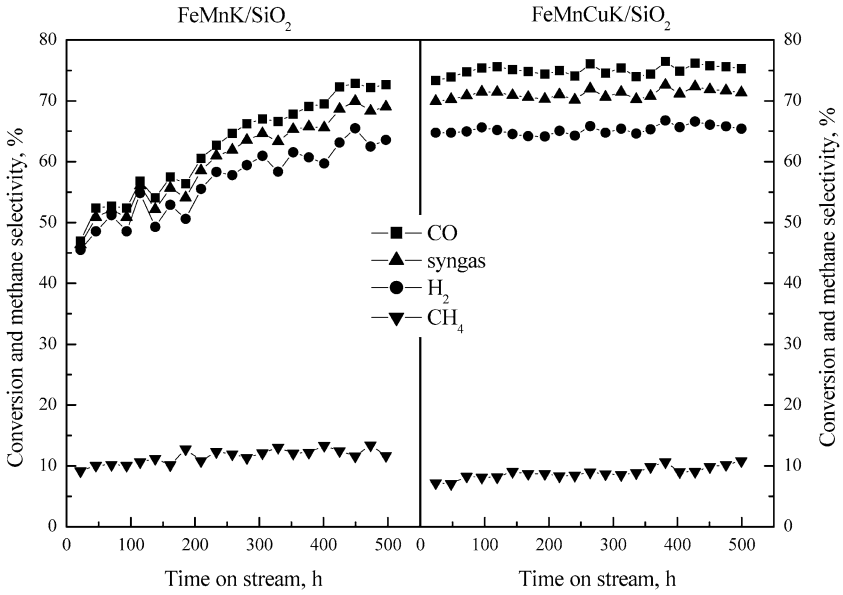

Fig. 8. Activity and stability of $FeMnK/SiO_2$ and $FeMnCuK/SiO_2$ catalysts; (■) CO conversion, (▲) syngas conversion, (●) H_2 conversion, (▼) methane selectivity; reaction conditions: 543 K, 1.5 MPa, 2000 h^{-1}, and $H_2/CO = 0.67$.

3.4.1. Activity and stability

Fig. 8 shows the conversions and stabilities for the FTS reaction (at pressurized conditions) of two catalysts during steady-state runs. The conversion of the $FeMnK/SiO_2$ catalyst increases slowly with time, whereas the conversion of the $FeMnCuK/SiO_2$ catalyst rapidly reaches a maximum and then levels off. Before approaching steady state, the activity of the $FeMnK/SiO_2$ catalyst shows a long (400 h) induction period, but that of the $FeMnCuK/SiO_2$ catalyst does not. After reaching steady-state activity, both catalysts show no difference in conversion. Clearly, copper decreases the time required to achieve steady-state activity but does not affect the final FTS activity.

As indicated by the H_2-TPR and CO-TPR findings and the reduction behavior, Cu can improve the reduction and increase the removal of oxygen in iron oxides under H_2 or CO. When exposed to syngas, copper oxide is first reduced by H_2 and CO to its metal state [14]. These metallic copper atoms, which are well dispersed in iron oxide phases, act as H_2 dissociation sites to provide activated H species or weaken the vicinal Fe–O bonds. Then the oxygen atoms in the Fe_2O_3 phase near the metallic Cu can be easily removed. Because the rates of reduction and carburization of an iron-based catalyst are typically controlled by the rate of oxygen removal [47], it is reasonable for the easier reduction and carburization of the $FeMnCuK/SiO_2$. The higher rate of reduction and carburization shortens the time for iron-phase transformation from Fe_2O_3 to Fe_3O_4 and FeC_x. This latter phase can provide a large number of FTS active sites on the crystallite surface. Thus, the induction period required to achieve steady-state activity is greatly shortened.

3.4.2. Selectivity

Both the catalyst and the reaction conditions influence FTS selectivity. Of all of the contributing factors, H_2/CO ratio has the strongest influence [48]. To correctly reflect the effect of the copper promoter on FTS selectivity, reaction experiments (after a 500-h run) were carefully conducted to obtain the results at identical H_2/CO and other conditions for the $FeMnK/SiO_2$ and $FeMnCuK/SiO_2$ catalysts (Table 4). As shown in Table 4, the selectivities to gaseous and light hydrocarbons (methane, C_2–C_4, and C_5–C_{11}) are suppressed, whereas those to heavy hydrocarbons (C_{12+} and especially C_{19+}) are enhanced with the addition of Cu into the catalyst ($FeMnCuK/SiO_2$). The $C_2^=$–$C_4^=/C_2^o$–C_4^o as a function of CO conversion and the olefin/paraffin as a function of carbon number are shown in Figs. 9 and 10, respectively. Both figures show that the ratio of olefin to paraffin is higher on the $FeMnCuK/SiO_2$ catalyst than on the $FeMnK/SiO_2$ catalyst. Fig. 9 also shows the variation of H_2/CO in tail gas as a function of CO conversion. The ratio of H_2 to CO is approximately identical on two catalysts, removing any influence of H_2/CO on selectivity. All of these results imply that the hydrogenation reaction is restrained and the chain propagation reaction is enhanced on the $FeMnCuK/SiO_2$ catalyst.

It is well known that increasing the surface basicity in a FTS catalyst can improve CO dissociative adsorption, suppress H_2 adsorption, facilitate chain growth reaction, and enhance selectivity to heavy hydrocarbons [8,10]. The results obtained in this study show that the Cu promoter obviously enhances FTS selectivity to heavier products. Recalling the results of CO_2 adsorption in the previous section, the FTS selectivity results reconfirm that basic sites existing on the catalyst surface of $FeMnCuK/SiO_2$ are responsible for the suppression of methane and other light-hydrocarbon products and the enhancement of the heavy products. Meanwhile, higher olefin selectivity is observed on the $FeMnCuK/SiO_2$ catalyst. The basic sites on the $FeMnCuK/SiO_2$ catalyst provide conditions for facilitating CO dissociation, leading to a relatively high coverage of carbon species on the surface, whereas insufficient hydrogen is present for a high paraffin production and/or chain termination rates.

Table 4
Hydrocarbon selectivity of $FeMnK/SiO_2$ and $FeMnCuK/SiO_2$ catalysts[a]

Catalysts	$FeMnK/SiO_2$				$FeMnCuK/SiO_2$			
H_2/CO exit ratio	0.75	0.77	0.80	0.82	0.74	0.78	0.79	0.93
H_2/CO utilized ratio	0.60	0.60	0.60	0.61	0.62	0.61	0.61	0.58
CO conversion (%)	59.0	64.9	69.8	74.6	62.1	65.9	68.00	76.2
H_2 conversion (%)	53.6	58.9	63.6	68.6	57.7	59.9	61.9	66.6
H_2 + CO conversion (%)	56.8	62.5	67.3	72.2	60.4	63.5	65.5	72.3
Hydrocarbon selectivity (wt%)								
CH_4	10.8	11.0	11.0	11.2	8.2	9.0	8.4	9.1
C_2–C_4	28.7	28.6	28.6	29.3	23.7	25.4	23.5	24.9
$C_2^=$–$C_4^=$	18.0	17.4	16.7	16.4	15.5	16.5	15.1	15.1
C_5–C_{11}	40.0	43.9	44.6	46.5	41.8	36.8	37.4	39.7
$C_5^=$–$C_{11}^=$	25.6	28.7	28.9	29.7	27.5	24.5	24.5	24.7
C_{12}–C_{18}	12.9	9.9	9.5	7.4	15.1	15.3	14.8	12.1
C_{19+}	3.2	1.6	1.7	1.0	9.0	11.5	13.8	12.3

[a] Reaction conditions: 543 K, 1.5 MPa, $H_2/CO = 0.67$, GHSV = 2000–4000 h^{-1} and reaction period = 500–800 h.

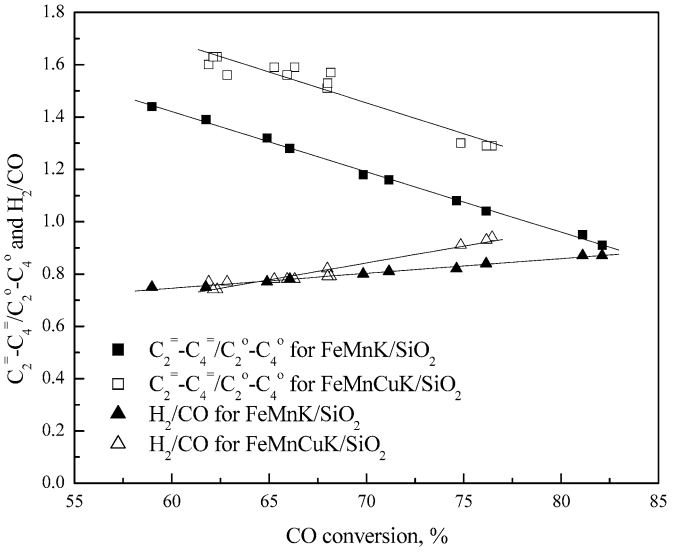

Fig. 9. $C_2^=$–$C_4^=/C_2^o$–C_4^o and H_2/CO ratios in tail-gas on $FeMnK/SiO_2$ and $FeMnCuK/SiO_2$ catalysts; reaction conditions: 543 K, 1.5 MPa, feed gas $H_2/CO = 0.67$, GHSV = 1500–4000 h^{-1} and reaction period = 500–800 h.

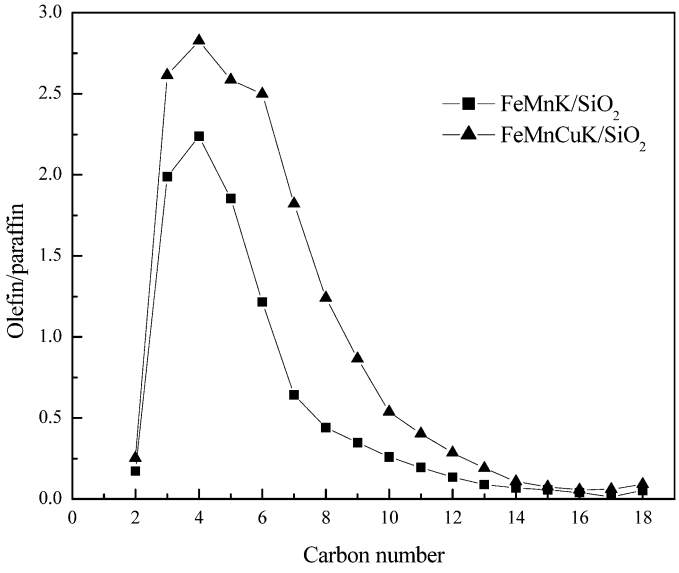

Fig. 10. Olefin/paraffin ratios as function of carbon number on (■) $FeMnK/SiO_2$ and (▲) $FeMnCuK/SiO_2$ catalysts (543 K, 1.5 MPa, H_2/CO = 0.67, and CO conversion of 75%).

It should not be forgotten that the Cu promoter might enhance the hydrogen activation on the surface, as is supported by the H_2-TPR/TPD studies given in Fig. 1 and Table 2. But for FTS reactions, the enhancement of hydrogen activation by the Cu promoter may not make up for the hydrogen consumption by the increased amount of carbon species due to the basic sites induced by the Cu promoter.

4. Conclusion

In this study, combined methods (TPR with DTG, TPD, and DRIFTS) were applied to characterize the metal oxide–support interaction on precipitated $FeMnK/SiO_2$ catalysts with and without copper promoter. Evidence for several kinds of interactions between metal elements and support, including iron–silica, copper–silica, and potassium–silica interactions, was found. In addition, a synergistic effect was observed on the Cu and K co-promoted catalyst ($FeMnCuK/SiO_2$), which has more surface basic sites than either of the separately Cu- and K-promoted catalysts ($FeMnK/SiO_2$ and $FeMnCu/SiO_2$).

The effect of Cu on reduction is to lower the reduction temperature and increase the reduction rate by the easy formation of metallic copper, acting as H_2 dissociation sites or weakening the vicinal Fe–O bonds, facilitating the removal of oxygen from the iron phase. The copper promoter also accelerates the carburization or the activation of catalyst in the CO or syngas atmosphere through copper's promotion of the reduction of iron oxides, whereas it does not affect the final extent of carburization.

In the FTS, Cu increases the initial conversions and shortens the induction period for reaching steady-state activity, but has no obvious effect on the steady-state conversions. Due to its higher surface basicity than the Cu-unpromoted catalyst ($FeMnK/SiO_2$), the $FeMnCuK/SiO_2$ catalyst has lower selectivity to methane and light hydrocarbons and enhanced selectivity to heavy hydrocarbons and olefins.

Acknowledgments

Financial support from the Chinese Academy of Sciences (KGCX1-SW-02), the National High Technology Research and Development Program of China (Program 863, 2001AA 523010), and the Key Program of National Natural Science Foundation of China (20590361) is gratefully acknowledged.

References

[1] M.E. Dry, Appl. Catal. A 276 (2004) 1.
[2] H. Kölbel, M. Ralek, Catal. Rev.-Sci. Eng. 21 (1980) 225.
[3] J. Barrault, C. Renard, Appl. Catal. 14 (1985) 133.
[4] M. Jiang, N. Koizumi, M. Yamada, J. Phys. Chem. B 104 (2000) 7636.
[5] Y. Yang, H. Xiang, Y. Xu, L. Bai, Y. Li, Appl. Catal. A 266 (2004) 181.
[6] Y. Yang, H.W. Xiang, L. Tian, H. Wang, C.H. Zhang, Z.C. Tao, Y.Y. Xu, B. Zhong, Y. Li, Appl. Catal. A 284 (2005) 105.
[7] Y. Yang, Ph.D. Dissertation, Institute of Coal Chemistry, CAS, 2004.
[8] M.E. Dry, G.J. Oosthuizen, J. Catal. 11 (1968) 18.
[9] M.E. Dry, T. Shingles, L.J. Boshoff, G.J. Oosthuizen, J. Catal. 15 (1969) 190.
[10] D.G. Miller, M. Moskovits, J. Phys. Chem. 92 (1988) 6081.
[11] T. Grzybek, J. Klinik, H. Papp, M. Baerns, Chem. Eng. Technol. 13 (1990) 156.
[12] S. Li, A. Li, S. Krishnamoorthy, E. Iglesia, Catal. Lett. 177 (2001) 197.
[13] S. Li, S. Krishnamoorthy, A. Li, G.D. Meitzner, E. Iglesia, J. Catal. 206 (2002) 202.
[14] Y. Jin, A.K. Datye, J. Catal. 196 (2000) 8.
[15] R.J. O'Brien, L. Xu, R.L. Spicer, S. Bao, D.R. Milburn, B.H. Davis, Catal. Today 36 (1997) 325.
[16] I.E. Wachs, D.J. Duyer, E. Iglesia, Appl. Catal. 12 (1984) 201.
[17] C.H. Zhang, B.T. Teng, Y. Yang, Z.C. Tao, Q.L. Hao, H.J. Wan, F. Yi, B.F. Xu, H.W. Xiang, Y.W. Li, J. Mol. Catal. A 239 (2005) 15.
[18] H.N. Pham, A.K. Datye, Catal. Today 58 (2000) 233.
[19] D.B. Bukur, X. Liang, D. Mukesh, W.H. Zimmerman, M.P. Rosynek, C. Li, Ind. Eng. Chem. Res. 29 (1990) 1588.
[20] D.B. Bukur, D. Mukesh, S.A. Patel, Ind. Eng. Chem. Res. 29 (1990) 194.
[21] S. Yuen, Y. Chen, J.E. Kubsh, J.A. Dumesic, N. Topsøe, H. Topsøe, J. Phys. Chem. 86 (1982) 3022.
[22] C.R.F. Lund, J.A. Dumesic, J. Phys. Chem. 85 (1981) 3175.
[23] I.R. Leith, M.G. Howden, Appl. Catal. 37 (1988) 75.
[24] J.O. Edstrom, J. Iron Steel Inst. 175 (1953) 289.
[25] M. Boudart, A. Delbouille, J.A. Dumesic, S. Khammouma, H. Topsøe, J. Catal. 37 (1975) 486.
[26] A.J.H.M. Kock, H.M. Fortuin, J.W. Geus, J. Catal. 96 (1985) 261.
[27] B.S. Clausen, H. Topsøe, S. Morup, Appl. Catal. 48 (1989) 327.
[28] S. Li, S. Krishnamoorthy, A. Li, G.D. Meitzner, E. Iglesia, J. Catal. 206 (2002) 202.
[29] M.E. Dry, T. Shingles, C.S. Van, H. Botha, J. Catal. 17 (1970) 341.
[30] X. Wang, G. Li, U.S. Ozkan, J. Mol. Catal. A 217 (2004) 219.
[31] F. Prinetto, G. Bhiotti, J. Phys. Chem. B 104 (2000) 11117.
[32] D. Bianchi, T. Chafik, M. Khalfallah, S.J. Teichner, Appl. Catal. A 105 (1993) 223.
[33] C. Schild, A. Wokaun, A. Baiker, J. Mol. Catal. 67 (1990) 223.
[34] N.D. Parkyns, J. Chem. Soc. A (1969) 410.
[35] Y.M. Grigoreev, D.V. Pozdnyakov, V.N. Filimonov, Russ. J. Phys. Chem. 46 (1977) 2.
[36] M.Y. He, J.G. Eckerdt, J. Catal. 87 (1984) 381.
[37] R. Brown, M.E. Cooper, D.A. Whan, Appl. Catal. 3 (1982) 177.
[38] A.J. Kock, H.M. Fortuin, J.W. Geus, J. Catal. 96 (1985) 261.
[39] I.S.C. Hughes, J.O.H. Newman, G.C. Bond, Appl. Catal. 30 (1987) 303.
[40] I.R. Leith, M.G. Howden, Appl. Catal. 37 (1988) 261.
[41] J.F. Shultz, W.K. Hall, T.A. Dubs, R.B. Anderson, J. Am. Chem. Soc. 78 (1956) 282.
[42] R. Dictor, A.T. Bell, J. Catal. 97 (1986) 121.
[43] K.R.P.M. Rao, F.E. Huggins, V. Mahajan, G.P. Huffman, V.U.S. Rao, B.L. Bhatt, D.B. Bukur, R.J. O'Brien, Top. Catal. 2 (1995) 71.
[44] L.D. Mansker, Y. Jin, D.B. Burker, A.K. Datye, Appl. Catal. A 186 (1999) 277.
[45] S. Li, G.D. Meitzner, E. Iglesia, J. Phys. Chem. B 105 (2001) 5743.
[46] D.B. Bukur, K. Okabe, M.P. Rosynek, C. Li, D. Wang, K.R.P.M. Rao, G.P. Huffman, J. Catal. 155 (1995) 353.
[47] S.T. Oyama, J.C. Schlatter, J.E. Metcalfe III, J.M. Lambert Jr., Ind. Eng. Chem. Res. 27 (1988) 1639.
[48] Y.Y. Ji, H.W. Xiang, J.L. Yang, Y.Y. Xu, Y.W. Li, B. Zhong, Appl. Catal. A 214 (2001) 77.